R. C. Bauer

AEDC-TR-74-5

SIMULATION OF FLOW APPROACHING THE CHIN INLET OF A RAMJET MISSILE

R. C. Bauer, W. W. Muse, and C. R. Tinsley
ARO, Inc.

ENGINE TEST FACILITY
ARNOLD ENGINEERING DEVELOPMENT CENTER
AIR FORCE SYSTEMS COMMAND
ARNOLD AIR FORCE STATION, TENNESSEE 37389

July 1974

Final Report for Period 1 July 1972 — 30 June 1973

Prepared for

ARNOLD ENGINEERING DEVELOPMENT CENTER (DYFS)
ARNOLD AIR FORCE STATION, TN 37389

NOTICES

When U. S. Government drawings specifications, or other data are used for any purpose other than a definitely related Government procurement operation, the Government thereby incurs no responsibility nor any obligation whatsoever, and the fact that the Government may have formulated, furnished, or in any way supplied the said drawings, specifications, or other data, is not to be regarded by implication or otherwise, or in any manner licensing the holder or any other person or corporation, or conveying any rights or permission to manufacture, use, or sell any patented invention that may in any way be related thereto.

Qualified users may obtain copies of this report from the Defense Documentation Center.

References to named commercial products in this report are not to be considered in any sense as an endorsement of the product by the United States Air Force or the Government.

APPROVAL STATEMENT

This technical report has been reviewed and is approved.

MARION L. LASTER
Research and Development
Division
Directorate of Technology

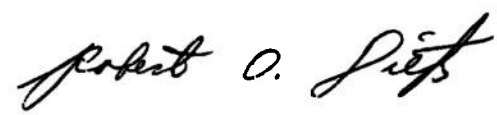

ROBERT O. DIETZ
Director of Technology

UNCLASSIFIED

SECURITY CLASSIFICATION OF THIS PAGE *(When Data Entered)*

REPORT DOCUMENTATION PAGE		READ INSTRUCTIONS BEFORE COMPLETING FORM
1. REPORT NUMBER AEDC-TR-74-5	2 GOVT ACCESSION NO.	3. RECIPIENT'S CATALOG NUMBER
4 TITLE *(and Subtitle)* SIMULATION OF FLOW APPROACHING THE CHIN INLET OF A RAMJET MISSILE		5. TYPE OF REPORT & PERIOD COVERED Final Report for Period 1 July 1972 - 30 Jun 1973 6. PERFORMING ORG. REPORT NUMBER
7. AUTHOR(s) R. C. Bauer, W. W. Muse, and C. R. Tinsley, ARO, Inc.		8. CONTRACT OR GRANT NUMBER(s) Program Element 65802F
9. PERFORMING ORGANIZATION NAME AND ADDRESS Arnold Engineering Development Center Arnold Air Force Station, Tennessee 37389		10 PROGRAM ELEMENT, PROJECT, TASK AREA & WORK UNIT NUMBERS
11 CONTROLLING OFFICE NAME AND ADDRESS Arnold Engineering Development Center (DYFS), Arnold Air Force Station, TN 37389		12. REPORT DATE July 1974 13. NUMBER OF PAGES 42
14. MONITORING AGENCY NAME & ADDRESS*(If different from Controlling Office)*		15. SECURITY CLASS. *(of this report)* UNCLASSIFIED 15a. DECLASSIFICATION/DOWNGRADING SCHEDULE N/A

16. DISTRIBUTION STATEMENT *(of this Report)*

Approved for public release; distribution unlimited.

17. DISTRIBUTION STATEMENT *(of the abstract entered in Block 20, if different from Report)*

18. SUPPLEMENTARY NOTES

Available in DDC.

19. KEY WORDS *(Continue on reverse side if necessary and identify by block number)*

altitude simulation	supersonic diffusers	drag
perfect gas simulation	jet engine inlets	
missiles	chin inlets	

20 ABSTRACT *(Continue on reverse side if necessary and identify by block number)*

A new Aerodynamic and Propulsion Test Unit (APTU) is being constructed at AEDC for testing air-breathing missiles that operate at supersonic Mach numbers. One type of missile configuration that may be tested in the APTU is that having a forward-located chin inlet. A technique for simulating the flow approaching a chin inlet is studied within the limitations of test body size, nozzle size, and diffuser performance expected in the APTU. Analytical techniques are presented for positioning

DD FORM 1 JAN 73 1473 EDITION OF 1 NOV 65 IS OBSOLETE

UNCLASSIFIED

SECURITY CLASSIFICATION OF THIS PAGE *(When Data Entered)*

20, Continued

the test body to obtain maximum altitude simulation and for estimating the general diffuser performance and starting conditions. A consideration of the flow processes that limit diffuser performance in a conventional test arrangement led to the concept of extending the diffuser over the test body. This concept was verified by small-scale experiments with the test body at 0- and 11-deg angles of attack and with the inlet open and closed. The diffuser extension was removed for one test configuration, and it was impossible to start the system within the test facility operating limits. Theoretical overall pressure ratios for diffuser starting and breakdown were about 16-percent conservative using a total drag coefficient of 1.0, based on the frontal area of the test body and support strut. The theoretical overall pressure ratio for breakdown was conservative by about 24 percent for the one configuration that exhibited a hysteresis effect on starting.

PREFACE

The work reported herein was conducted by the Arnold Engineering Development Center (AEDC), Air Force Systems Command (AFSC), Arnold Air Force Station, Tennessee. The results were obtained by ARO, Inc. (a subsidiary of Sverdrup & Parcel and Associates, Inc.), contract operator of AEDC, AFSC. The work was conducted under ARO Project No. RF210, and the manuscript (ARO Control No. ARO-ETF-TR-73-143) was submitted for publication on November 8, 1973.

CONTENTS

ILLUSTRATIONS

Figure

APPENDIXES

1.0 INTRODUCTION

A new Aerodynamic and Propulsion Test Unit (APTU) is being constructed at AEDC for testing air-breathing missiles that operate at supersonic Mach numbers in the altitude range from sea level to about 90,000 ft. The test facility is of the blow-down type, having a diffuser system consisting of a 4-ft-diam duct connected to a 5-ft-diam duct that exhausts to the atmosphere. Each diffuser has a length-to-diameter ratio of about 8.0 with an annular jet pump located at the junction of the 4- and 5-ft ducts. The jet pump is used to assist in obtaining high altitude test conditions.

Ramjet-powered missiles can be characterized by the location of the engine inlets. Simulation of flow approaching aft-located inlets was studied in Ref. 1. In this report, simulation of flow approaching a forward-located "chin" inlet is studied within the limitations on mass flow and diffuser performance expected in the APTU facility. The major problem areas considered are (1) test body position, (2) diffuser performance, and (3) hysteresis effects on diffuser starting, for test body angles of attack of 0 and 11 deg.

2.0 ANALYSIS

A sketch of the system to be analyzed is presented in Fig. 1. The analysis is divided into two parts, (1) general performance and (2) starting conditions. The general performance analysis determined the relationships between the nozzle total pressure, p_{t_N}, the chamber pressure, p_c, and the exhaust pressure, p_B. The starting conditions analysis relates the nozzle total pressure, p_{t_N}, to the maximum chamber pressure, $(p_c)_S$, at which the system will operate in a steady-state started condition (see Section 2.2). A combination of the two analyses can be used to relate the nozzle total pressure, p_{t_N}, to the maximum exhaust pressure, $(p_B)_S$, at which the system will operate in its started condition. A detailed development of each analysis is presented in the following sections.

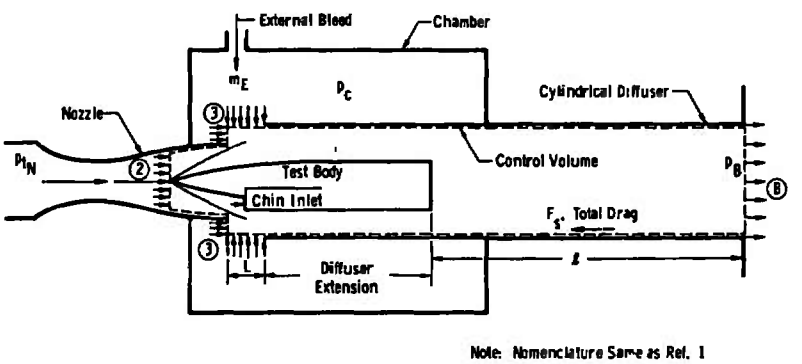

Figure 1. Sketch of test cell.

2.1 GENERAL PERFORMANCE ANALYSIS

The equations describing the general diffuser performance are derived by applying the fluid mechanical conservation laws to the control volume shown in Fig. 1. The conservation laws are applied based on the following assumptions:

1. The test facility nozzle provides one-dimensional supersonic flow approaching the test vehicle. This is necessary for proper flow simulation.

2. The bow shock wave from the test vehicle falls outside the facility nozzle exit; therefore, the total stream thrust on control volume surface 2 equals the total stream thrust that would exist at the nozzle exit plane without the presence of the test vehicle.

3. The flow conditions over surface 3 of the control volume are one-dimensional.

4. The flow field within the chamber is the low velocity, recirculating type; thus, the chamber pressure, p_c, is the total pressure of the flow on surface 3 of the control volume.

5. All the gases are perfect.

6. The cylindrical diffuser is of sufficient length to allow complete mixing; therefore, the flow conditions at the diffuser exit (surface B of the control volume) are one-dimensional.

7. There are no regions of flow separation in the facility nozzle.

8. The test vehicle engine is not operating. (Engine-on operation can be computed by the more general control volume analysis presented in Ref. 1.)

Based on these assumptions, the basic equations for steady flow are as follows:

Conservation of Mass Flow:

$$m_2 + m_3 = m_B$$

also

$$m_3 = m_E$$

Conservation of Momentum (X-direction):

$$F_2 + F_3 - F_S = F_B$$

Conservation of Energy:

$$m_2 C_{p_2} T_{t_2} + m_3 C_{p_3} T_{t_3} = m_B C_{p_B} T_{t_B}$$

also

$$m_3 C_{p_3} T_{t_3} = m_E C_{p_E} T_{t_E}$$

In practice, limitations to this analysis are imposed by boundary-layer separation, diffuser choking, jet pluming, and base flow phenomena. Assumption number 7 is valid only if the ratio of chamber pressure, p_c, to nozzle exit pressure, p_N, does not exceed the nozzle boundary-layer separation pressure ratio. This determines the maximum chamber pressure at which the nozzle will flow full. The minimum chamber pressure, p_c, is determined by either diffuser choking, jet pluming, or base flow phenomena. Diffuser choking can occur on control volume surfaces 3 and B and is predictable by the control volume analysis. The accuracy of the predicted diffuser choking depends strongly on the accuracy of the estimated drag of the test vehicle. Limitations caused by either jet pluming or base flow phenomena are illustrated in Figs. 2a and b without the presence of a test vehicle. The jet pluming limitation occurs when the diffuser inlet is located a significant distance downstream of the nozzle exit, depending on the diffuser size. By applying conservation of mass flow to the test chamber, one finds that the minimum chamber pressure is that which produces a plume diameter equal to the diffuser diameter at the diffuser entrance. The plume can be computed for axisymmetric inviscid flow by the well-known method of characteristics solution technique applied to the general potential flow equations. Mixing along the plume boundary tends to increase the effective plume diameter; thus the theoretical inviscid minimum chamber pressure will be less than the experimental pressure.

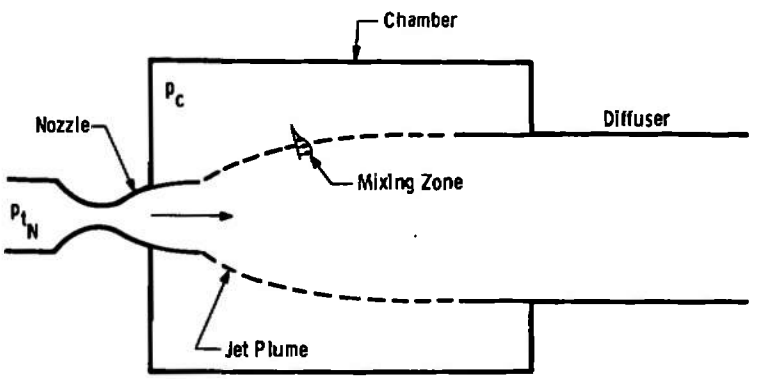

a. Jet plume limit

Figure 2. Limits on minimum chamber pressure.

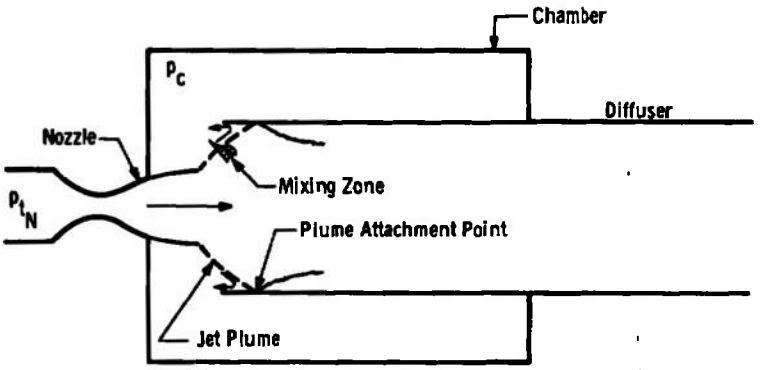

b. Base flow limit

Figure 2. Concluded.

The chamber pressure will decrease as the distance between the nozzle exit and the diffuser entrance is decreased. The plume will begin to attach itself to the internal surface of the diffuser, and a base flow type of phenomenon will be established as shown in Fig. 2b. The minimum chamber pressure occurs when the diffuser entrance is sufficiently far upstream of the plume attachment point that it will not interfere with the recompression process. The minimum chamber pressure for axisymmetric flow can be estimated by applying the Korst base pressure theory, as in Ref. 2. It is important to note that the minimum chamber pressure produced by the base flow limit is significantly less than that produced by the pluming limit.

The major effect of the test vehicle on the jet plume and base flow limits is caused by a distortion of the plume shape; this distortion usually results in an increase of the minimum test cell pressure. For a nonaxisymmetric test vehicle at a finite angle of attack, the plume boundary surface is three-dimensional and cannot be theoretically predicted using existing analytical techniques. Therefore, to be sure that the minimum chamber pressure will be the lowest possible. the diffuser should extend over the test vehicle so that the base flow limit occurs. However, when this is done the flow area blockage between the test vehicle and the diffuser extension should not exceed the well-known normal shock limits.

In summary, the range of applicability of this analysis can be represented as follows:

$$1. \quad \left(\frac{P_c}{P_N}\right)_{MIN} \leq \left(\frac{P_c}{P_N}\right) \leq \left(\frac{P_c}{P_N}\right)_{\substack{BLS \\ (MAX)}}$$

2. $M_3 \leq 1.0$

3. $M_B \leq 1.0$

2.2 STARTING CONDITIONS ANALYSIS

A diffuser system is understood to be operating in a started condition when there are no disturbances influencing the test body flow field of interest. In this study, the flow field of interest is that approaching the chin inlet of the test vehicle. The major source of disturbance to this flow field will emanate from the nozzle exit because of a difference in pressure between the chamber, p_c, and the nozzle exit, p_N. However, disturbances can also be produced by excessive blockage (exceeding the normal shock limit) between the test body and the nozzle or diffuser extension, thus preventing the establishing of supersonic flow. Usually these disturbances can be eliminated by moving the test body to a position of low blockage to allow the flow to become supersonic and then returning the body to its original position. For marginal blockage configurations, it is sometimes possible to establish supersonic flow by decreasing the chamber pressure, p_c, to a relatively low level so that it can then be increased without breaking down the supersonic flow. This is referred to as a hysteresis effect on starting conditions and, at the present time, can be determined only by experiment.

Assuming that disturbances caused by blockage are eliminated by properly sizing the nozzle and diffuser, then the only source of disturbance is that caused by the chamber pressure, p_c. If the chamber pressure is less than the nozzle exit pressure, the flow expands at the nozzle exit and the test rhombus is defined by Mach lines as shown in Fig. 3. The upstream Mach lines are determined by the nozzle contour and are independent of the chamber pressure if the nozzle is always flowing full. The downstream Mach lines originate upstream of the nozzle exit because of the feedback effect which results in the acceleration of the boundary layer near the nozzle exit when $p_c < p_N$. The maximum feedback distance is about five boundary-layer thicknesses, based on the experimental data presented in Ref. 3.

In most practical tests the chamber pressure will be limited to a value greater than the nozzle exit pressure, and oblique shock waves will form the downstream boundaries of the test rhombus as shown in Fig. 3. For the maximum chamber pressure allowed by boundary-layer separation, the shock waves originate upstream of the nozzle exit a distance of two and one-half (2.5) boundary-layer thicknesses, based on the experimental data presented in Ref. 3. The angle of the shock wave far from the nozzle centerline can be computed from two-dimensional shock wave theory since the static pressure ratio across the shock wave equals the known ratio of chamber pressure to nozzle exit pressure.

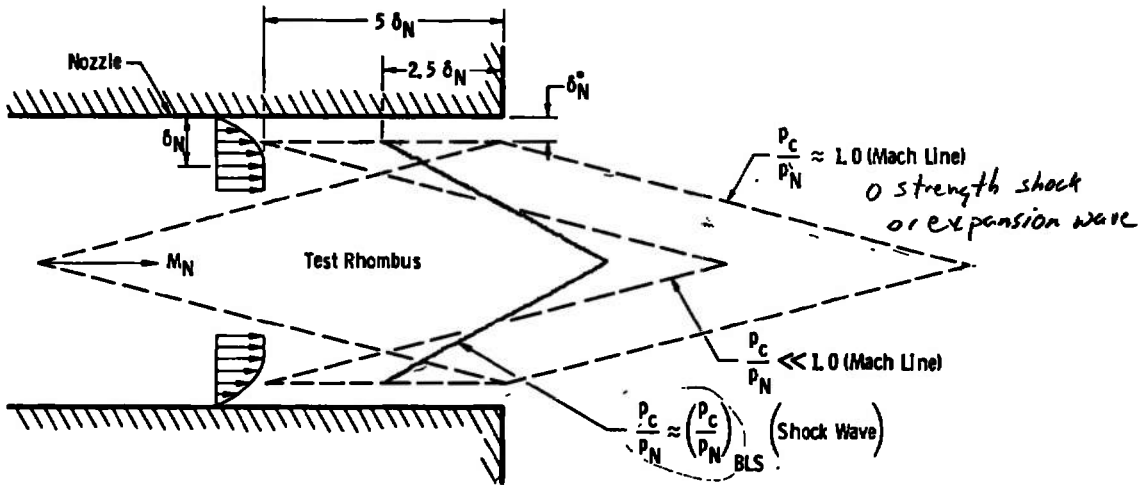

Figure 3. Variation of test rhombus with chamber pressure.

For chamber pressures less than the maximum allowed by boundary-layer separation, the shock waves are assumed to originate a distance upstream of the nozzle exit equal to one-half the total distance the pressure will feed back in the nozzle boundary layer. A simple method for estimating the pressure feedback distance is presented in Ref. 1.

The location of the test body in the test rhombus determines the starting chamber pressure, $(p_c)_S$. The test vehicle should be located within the test rhombus determined by the maximum chamber pressure allowed by boundary-layer separation to increase the probability that a given test configuration will start. The reason for this is that, for a given test configuration, the minimum chamber pressure that will be established is unknown a priori.

2.3 OVERALL STARTING PRESSURE RATIO

The overall starting pressure ratio, $(p_B)_S/p_{t_N}$, is determined by combining the General Performance Analysis with the Starting Conditions Analysis previously described. Since the General Performance Analysis presented in this report is a simplification of the analysis presented in Ref. 1, the computer program developed for Ref. 1 was used in this study. Computer inputs for a sample calculation are presented in Appendix A to illustrate the various assumptions necessary to apply the more general analysis to the type of diffuser system of interest in this study. The sample calculation is an application of the analysis to the experimental configuration described in the following section.

3.0 EXPERIMENTAL STUDY

3.1 OBJECTIVE

The purpose of this study was to provide experimental data for evaluation of the theoretical analysis. In particular, it was of interest to determine the starting characteristics and minimum chamber pressure for a typical test arrangement expected in the full-scale APTU facility.

3.2 EXPERIMENTAL APPARATUS

3.2.1 Basic Facility

The tests were conducted in the Pilot Test Unit (PTU). The PTU is a scale model of the large APTU facility, and its operation is similar in that it is of the blowdown type, exhausting to atmosphere with temperature established by a stored energy heater. The basic PTU geometry and performance are described in Appendix B.

3.2.2 Test Cell

A sketch of the test cell is presented in Fig. 4, defining the nozzle, test chamber, and diffuser system. The nozzle contour was designed for heated air (γ_N = 1.38) by the method of characteristics to produce uniform exit flow conditions. The nozzle contour was corrected for boundary-layer growth by Tucker's method (Ref. 4) based on a nozzle total pressure of 270 psia and a total temperature of 1460°R. The maximum operating conditions of the facility are (1) a total pressure of 400 psi and (2) a total temperature of 1460°R.

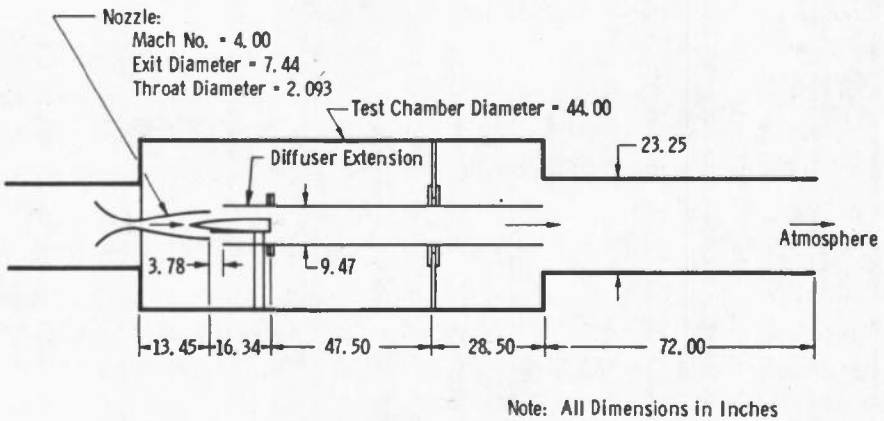

Figure 4. Sketch of experimental test cell.

The basic test body is the same one used in the study presented in Ref. 1 but is modified to include a chin engine inlet as shown in Fig. 5. The exit of the inlet could be blocked to simulate a no-flow condition. The basic test body is 3.5 in. in diameter and has a 2.92 von Kármán forebody.

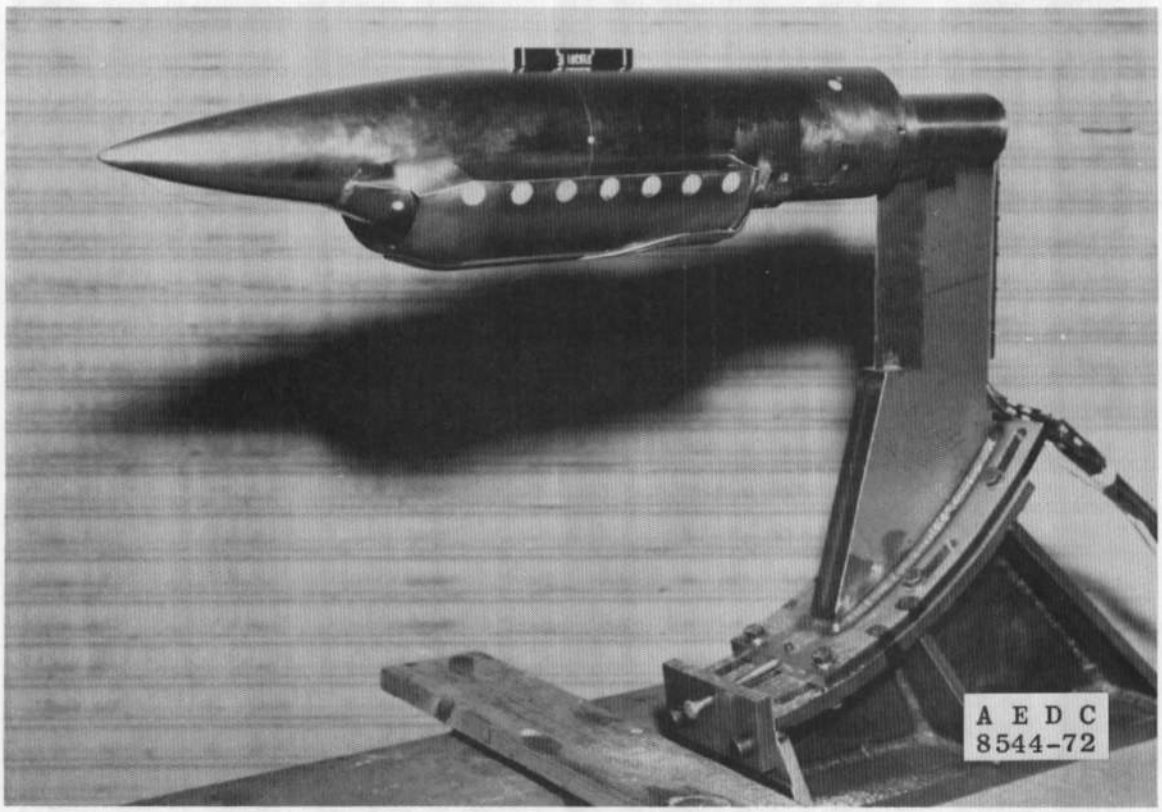

Figure 5. Test body and support strut.

The nozzle, test body, and diffuser are a 0.2067 scale model of a typical test arrangement expected in the full-scale APTU facility.

The position of the test body relative to the nozzle was determined by first computing the bow shock from the test body for the two desired test body angles of attack of 0 and 11 deg. This was done by the analytical technique presented in Ref. 5. The next step was to determine the nozzle test rhombus allowed by boundary-layer separation. The boundary-layer separation pressure ratio was assumed equal to the nozzle Mach number, as in Ref. 1. The shock wave angle that bounds the downstream edges of the

test rhombus was computed from two-dimensional shock wave theory. The equation is as follows:

$$\sin^2\theta = \frac{1}{M_N}$$

This shock wave emanates from the boundary-layer displacement thickness contour a distance of 2.5 δ_N upstream of the nozzle exit, as illustrated in Fig. 3. The boundary-layer thicknesses were those used to design the nozzle contour. A sketch of the test body position selected for zero angle of attack is shown in Fig. 6a. The test body is located in the downstream portion of the test rhombus and above the nozzle centerline in an attempt to force the flow boundary to attach to the diffuser internal surface, thus establishing a base flow type of limit on diffuser performance. Tests were conducted with the test body at two vertical positions at an 11-deg angle of attack. At the highest vertical position, as shown in Fig. 6b, the bow shock wave on the leeward side of the test body impinges on the nozzle exit corner. In the lower position, the bow shock wave on the leeward side passes through the edge of the boundary layer.

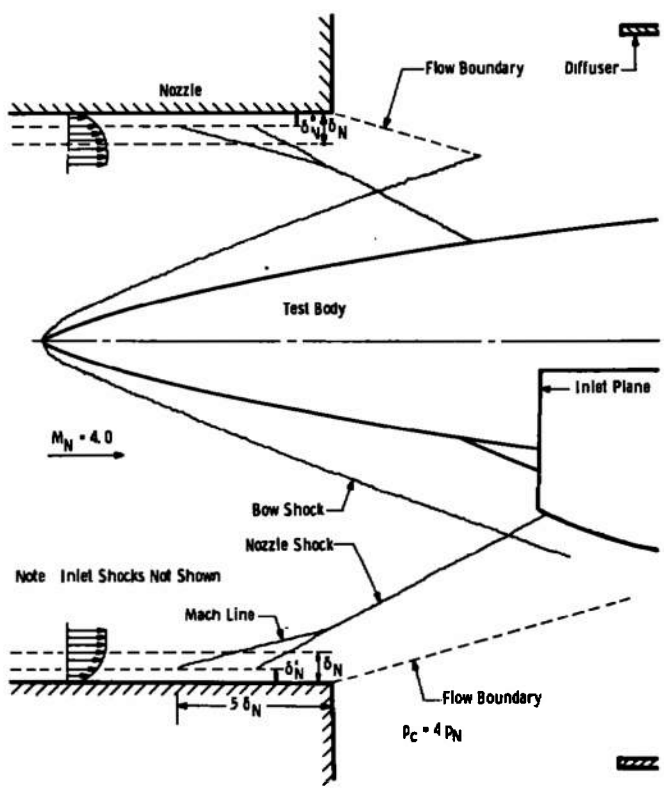

a. $\alpha = 0$

Figure 6. Test body position.

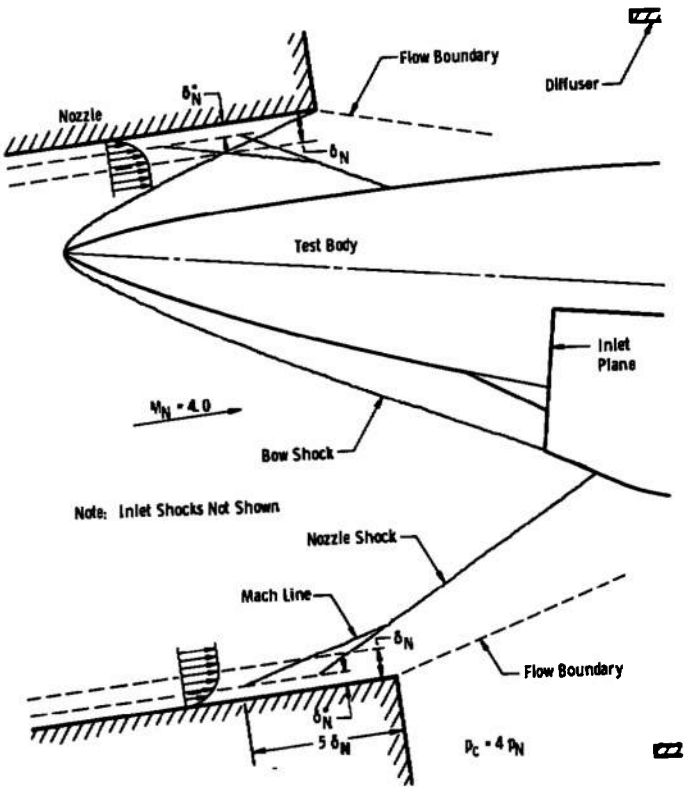

b. α = 11 deg

Figure 6. Concluded.

The test body was sting supported from a vertical strut that passed through the bottom of the diffuser. The strut was aerodynamically shaped to reduce drag and had a frontal area equal to about 14 percent of the test body frontal area. Tests were conducted with and without various leakage areas at the strut/diffuser junction.

3.2.3 Instrumentation

The parameters measured were as follows:

1. Nozzle total pressure, p_{t_N}
2. Nozzle total temperature, T_{t_N}
3. Chamber pressure, p_c
4. Test body static pressures, p_M
5. Diffuser static pressures, p_D

The pressures were measured with strain-gage-type transducers. The transducers were shunt resistance calibrated in the laboratory, and the data acquisition system (including the transducers) was resistance calibrated before and after each test period. The temperature recording system was millivolt calibrated before each test period.

3.2.4 Data Acquisition

All pressure and temperature data were recorded on a computer-controlled Digital Data Acquisition System (DDAS). All data obtained on the DDAS were recorded on magnetic tape in digital form at a scan rate of 20,000 channels/sec. Reduced data were obtained in the off-line mode of operation. The estimated accuracy of the pressure data is ±0.5 percent for steady-state operation. The theoretical transient response time of each pressure-measuring system was less than 1 sec to measure within 1 percent of the true value. The accuracy of the temperature data is ±2°F.

3.3 EXPERIMENTAL PROCEDURE

The PTU is a blowdown type of facility having an average run time of about 5 min for these tests. The data were obtained by increasing the nozzle total pressure to a maximum of about 400 psia and then decreasing the total pressure. With this test procedure it was possible to determine the complete diffuser performance and establish the possible existence of hysteresis.

4.0 EVALUATION OF THEORY

4.1 APPLICATION OF THEORY

The General Performance Analysis and the Starting Conditions Analysis apply if the establishment of supersonic flow is not limited by test body blockage. The maximum flow contraction is at the nozzle exit and is 0.92 for the experimental configuration described in Fig. 4. The maximum flow contraction allowed by normal shock wave theory is 0.676; so for a flow Mach number of 4.0, there should be no effect of test body blockage on diffuser starting.

The General Performance Analysis was applied to the experimental configuration shown in Fig. 4 by using the computer program developed for the more general control volume analysis presented in Ref. 1. Inputs for this computer program are presented in Appendix A.

4.2 COMPARISON OF THEORY WITH EXPERIMENTS

4.2.1 Without Test Body

The theoretical general diffuser performance for zero drag coefficient is compared with experiment in Fig. 7. The theory is based on steady flow, but the experimental

data were obtained by a transient test procedure. The good agreement of the theory with experiment indicates that the experimental data may be treated as steady state. The experimental minimum chamber pressure ratio, p_c/p_{t_N}, is shown in Fig. 7 to agree well with the theoretical jet pluming limit. The theoretical base pressure limit is estimated to be about half the experimental value.

Comparing the data obtained for increasing total pressure (open symbols) with that obtained for decreasing total pressure (closed symbols) shows that there are no significant hysteresis effects on the performance of this system.

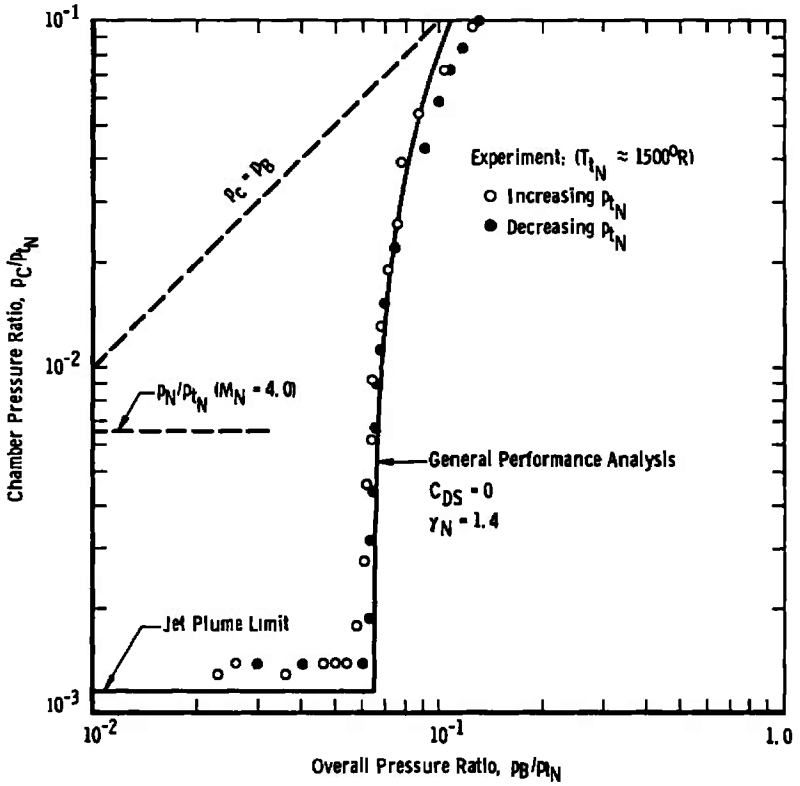

Figure 7. General diffuser performance without test body.

4.2.2 Test Body at Zero Angle of Attack

In Fig. 8 the theory is compared with experimental data obtained with the engine inlet open and closed. The experimental data agree well with the theory for zero drag, indicating that the wave drag is being reduced by the diffuser extension. The major effect of the test body is to significantly increase the minimum chamber pressure. The experimental data for the inlet-open configuration indicates a significant hysteresis effect on diffuser performance. However, the abrupt decrease in the minimum chamber pressure

indicates the possibility of a test chamber leak that sealed itself during the test run. Unfortunately, time did not permit a repeat test of this configuration. The experimental data for the inlet-closed configuration indicate that there are no significant hysteresis effects on diffuser performance.

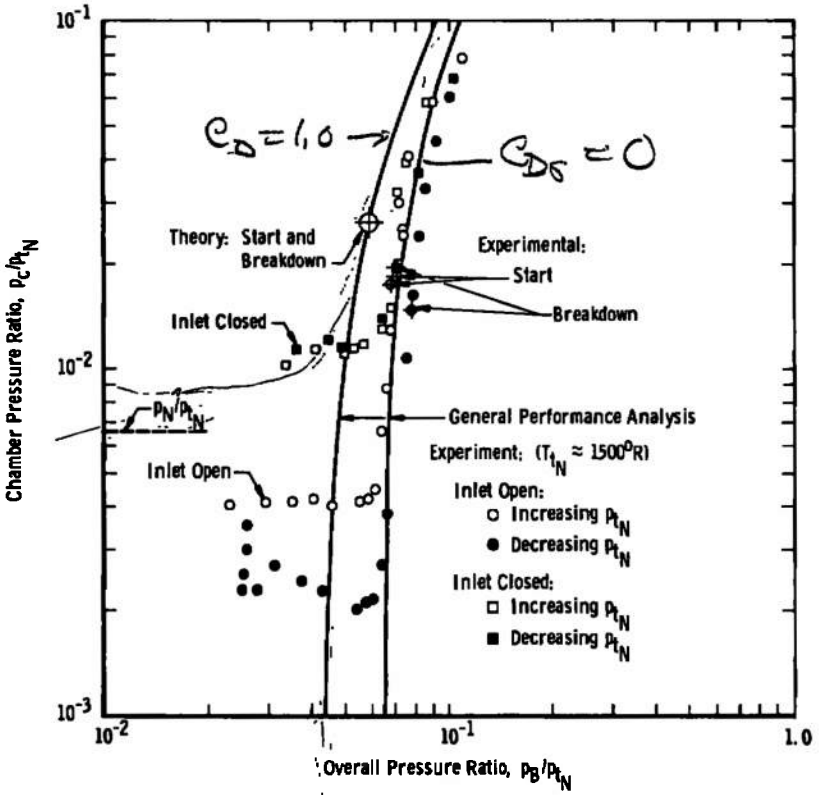

Figure 8. General diffuser performance with test body at zero angle of attack.

The most important experimental result is the determination that for both inlet configurations the minimum chamber pressure is much less than the assumed value for nozzle bounday-layer separation; therefore, the system should be started. To determine when the system becomes started, it is necessary to consider the static pressure distribution on the test body as shown in Figs. 9a and b for zero angle of attack. The system is defined as started when there are no disturbances influencing the flow approaching the engine inlet. The static pressure distribution on the test body was used to indicate when the system became started. Experimental data are compared with theory in Fig. 9a for the inlet-open configuration. Analysis of the experimental data indicated a bias because of time lag in the pressure-measuring system. This time lag was most significant during the start-up and shut-down periods of the test run. Unfortunately, the diffuser became started and unstarted during these time periods, making it impossible to determine the

precise conditions at which the diffuser became started. The experimental data presented in Fig. 9a for a nozzle total pressure, p_{t_N}, of 400 psia are considered steady-state data since this test condition was maintained for about 18 sec. The good agreement of these data with the theoretical pressure distribution upstream of the inlet verifies the design and fabrication of the nozzle for this application, since this pressure distribution is highly sensitive to nonuniformities in the approaching flow field. The nozzle was not calibrated prior to these tests because diffuser performance is not measurably affected by small disturbances produced by fabrication errors.

The diffuser starting conditions were determined based on maintaining a decreasing nondimensional static pressure distribution on the test body upstream of the engine inlet. The pressure distribution through the inlet is not a good indicator of the type of flow conditions approaching the inlet since the flow through the inlet can be a strong function of the exterior pressure at its exit. The shape of the pressure distribution on the test body nose was used to determine starting conditions since the absolute level is believed to be biased by the time lag of the measuring system. The pressure distributions for starting and breakdown are presented in Fig. 9a. The system becomes started at a nozzle total pressure of 201 psia and an overall pressure ratio, p_B/p_{t_N}, of 0.0685 and breaks down at a nozzle total pressure of 178 psia and an overall pressure ratio, p_B/p_{t_N}, of 0.0777. The corresponding ratios of chamber pressure to nozzle exit static pressure, p_c/p_N, are 2.81 and 2.26. The experimental overall pressure ratios for starting and breakdown are 56 and 64 percent of the normal shock value for a Mach number of 4.0. The corresponding simulated altitudes are 55,000 and 57,800 ft. The theoretical overall pressure ratio, p_B/p_{t_N},

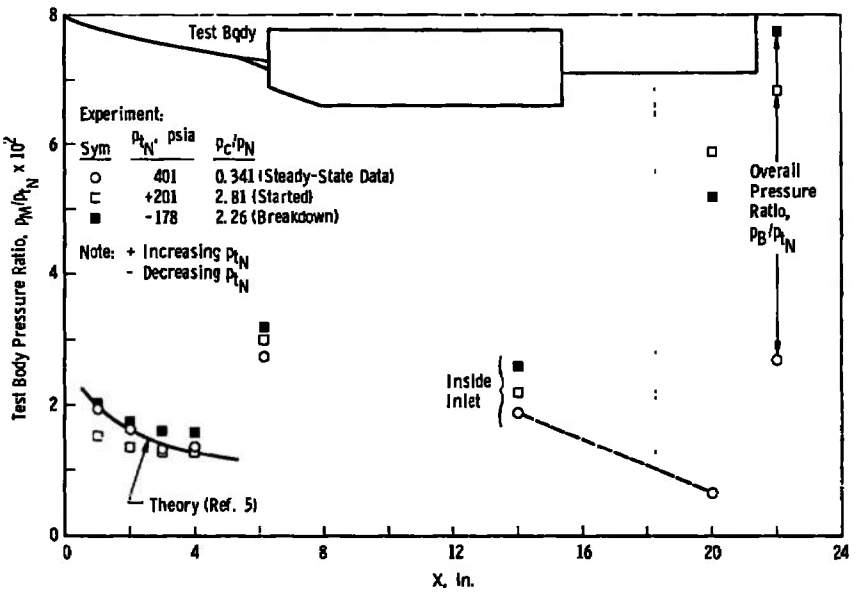

a. Inlet open

Figure 9. Test body pressure distributions at zero angle of attack.

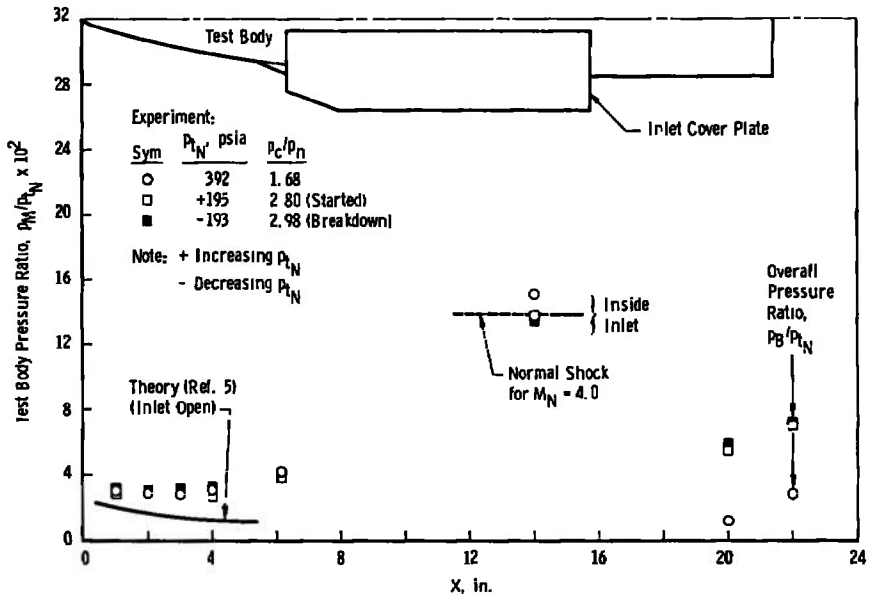

b. Inlet closed

Figure 9. Concluded.

for starting is 0.0591 based on a drag coefficient, C_{DS}, of 1.0 (reference area is frontal area of test body plus support strut) and a ratio of 4.0 for p_c/p_N. The theory is conservative in predicting the overall pressure ratio for starting by about 14 percent and for breakdown by 24 percent. The accuracy of the theory could be improved by a reliable estimate of the total drag coefficient, C_{DS}. However, the complexity of the flow field makes such an estimate impossible at the present time.

In Fig. 9b experimental data are compared with the theory for the inlet-closed configuration. The inlet was closed by a cover plate at its exit. The data indicate that the flow is separated from near the nose of the test body back to somewhere in the inlet. The maximum pressure inside the inlet is shown in Fig. 9b to be approximately equal to the total pressure downstream of a normal shock wave at a Mach number of 4.0. This indicates that the separated flow is reattaching to the inlet ramp rather than the outside lip. The maximum pressure inside the inlet (Sta. 14) was used to indicate when the system became started and unstarted. The reference pressure was the theoretical normal shock pressure based on a Mach number of 4.0. The system becomes started at a nozzle total pressure of 195 psia and an overall pressure ratio, p_B/p_{t_N}, of 0.0703 and breaks down at a nozzle total pressure of 193 psia and an overall pressure ratio of 0.0708. The corresponding ratios of chamber pressure to nozzle exit static pressure, p_c/p_N, are 2.80 and 2.98. The theoretical overall pressure ratio is the same as for the inlet-open configuration and is conservative by about 16 percent for both starting and breakdown. The theory is in better agreement with these data than with the inlet-open configuration, primarily because of the lack of a hysteresis effect on diffuser performance.

4.2.3 Test Body at 11 deg Angle of Attack

The general diffuser performance with the test body at 11 deg angle of attack is presented in Fig. 10. Data presented are with the diffuser extension installed (Fig. 4) for the following configurations: 1) inlet open and closed; 2) test body at its upper and lower positions, and without the diffuser extension for the inlet-open configuration. The upper position of the test body is shown in 6b, and the lower position was obtained by vertically translating the test body downward 0.25 in. All aspects of the experimental data were identical for the two test body positions. This is verified in Fig. 10 for the general diffuser performance. The major effect of test body angle of attack on the general diffuser performance was to increase the minimum chamber pressure ratio, p_c/p_{t_N}, by nearly a factor of 2.0 over that for zero angle of attack. However, the minimum chamber pressure ratio for both the inlet-open and -closed configurations was low enough to allow the system to become started. The expected increase in test body drag caused by angle of attack apparently did not occur, as indicated in Fig. 10 by the good agreement of the data with the theory for zero drag. Apparently compression disturbances from the

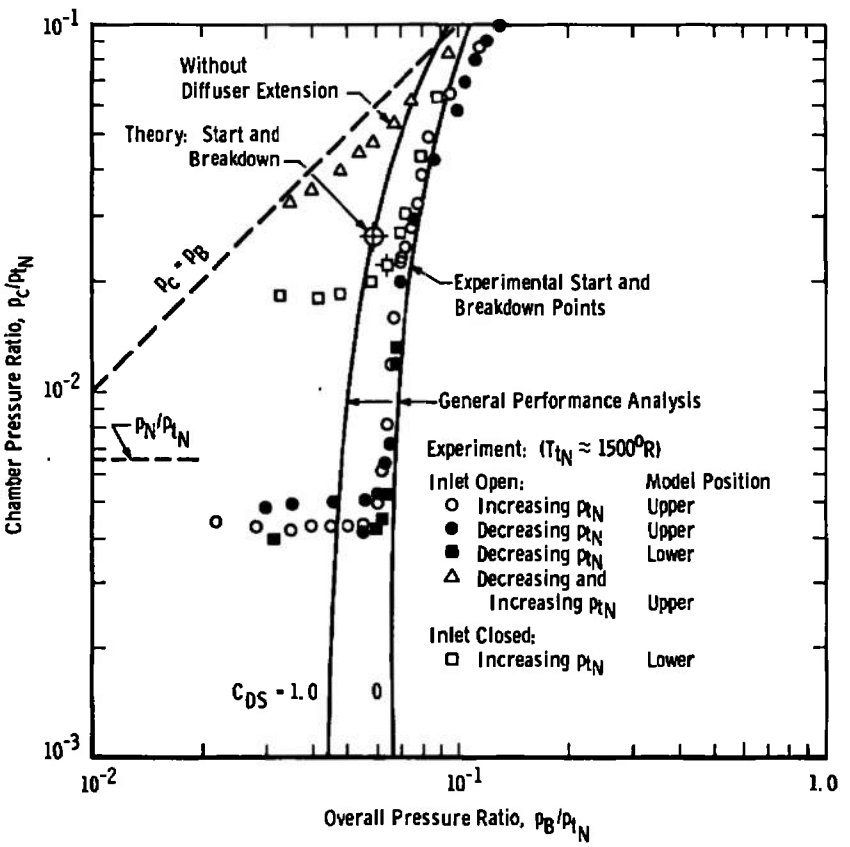

Figure 10. General diffuser performance with test body at 11 deg angle of attack.

diffuser extension increase the static pressure on the rear portions of the test body, thus reducing the wave drag. Or it may be that the test body produces a second throat effect that would appear to be a reduction in test body drag. Whatever the cause, this is a very desirable additional effect produced by the diffuser extension since the main purpose of the diffuser extension is to produce a base flow limit on the minimum chamber pressure ratio, p_c/p_{t_N}. Experimental data obtained without the diffuser extension show that the minimum chamber pressure ratio, p_c/p_{t_N}, is about ten times that obtained with the diffuser extension. As a result, the system never became started.

The nondimensional static pressure distributions on the test body for the inlet-open and -closed configurations are presented in Figs. 11a and b. The starting conditions were determined based on maintaining a decreasing static pressure distribution on the test body upstream of the engine inlet as was done for the zero angle-of-attack tests. The experimental static pressure distributions on the test body for the inlet-open configuration are presented in Fig. 11a for the maximum nozzle total pressure during the test run of 400 psia and for nozzle total pressures of 197 and 193 psia, corresponding to starting and breakdown. The overall pressure ratios, p_B/p_{t_N}, for starting and breakdown are 0.0698 and 0.0707; and the ratios of chamber pressure, p_c, to nozzle exit static pressure, p_N, are 3.42 and 3.54. The theoretical overall pressure ratios for starting and breakdown are the same as for the zero angle-of-attack configuration and are conservative by about 15 percent for starting and 16 percent for breakdown.

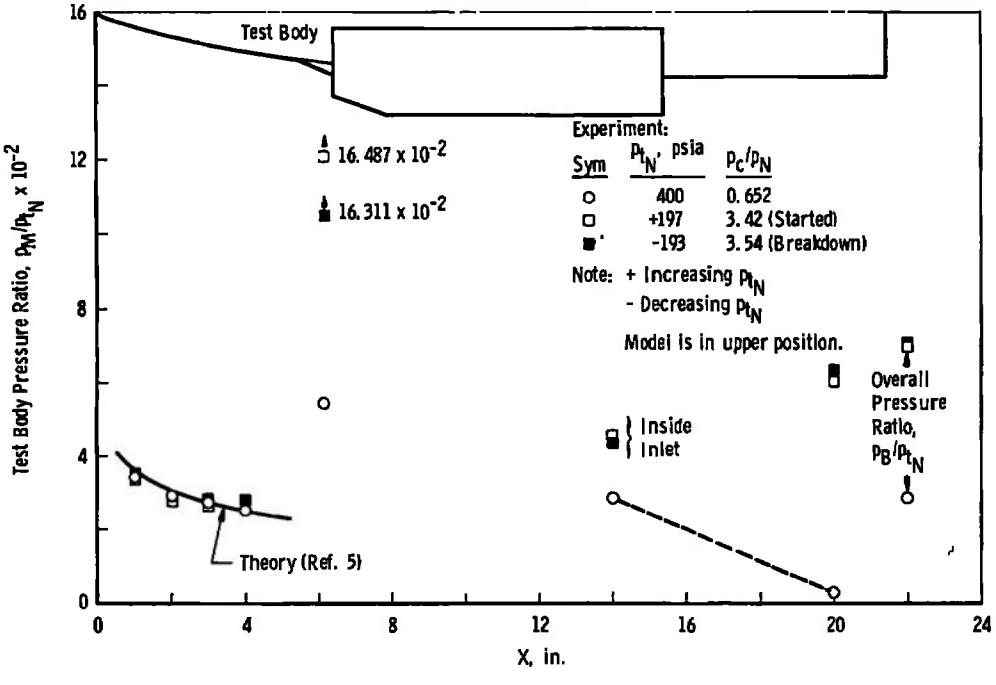

a. Inlet open

Figure 11. Test body pressure distributions at 11 deg angle of attack.

The inlet cover plate broke off during the test run for the inlet-closed configuration, making it impossible to determine the conditions for diffuser breakdown. The cover plate broke at a nozzle total pressure of 381 psia, and the corresponding static pressure distribution on the test body is presented in Fig. 11b. The maximum pressure inside the inlet, as shown in Fig. 11b, is approximately two times that predicted by normal shock wave theory for a Mach number of 4.0. The maximum pressure for zero angle of attack was approximately equal to the normal shock pressure. The data presented in Fig. 11b also show that the flow is attached to the test body from its nose to almost the ramp of the inlet. The flow was separated throughout this region for zero angle of attack.

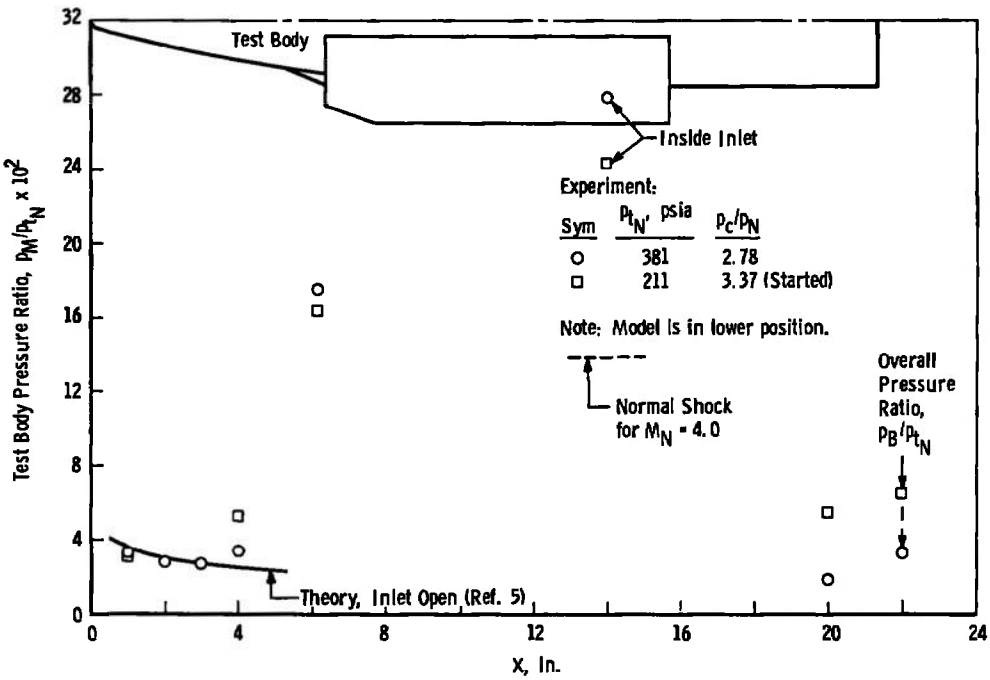

b. Inlet closed

Figure 11. Concluded.

Diffuser starting for the inlet-closed configuration was assumed to occur at the same ratio of chamber pressure to nozzle exit static pressure as for the inlet-open configuration. This starting criterion was selected because it was not possible to use the normal shock pressure as was done for the zero angle-of-attack configuration. In addition, for a practical engine test it is important for the system to remain started during the transition from engine-off to engine-on, so the facility conditions must be set for the more severe starting conditions. Based on these criteria, the nozzle total pressure for starting is 211 psia, and the overall pressure ratio, p_B/p_{t_N}, is 0.0644. The theoretical overall pressure ratio is conservative by about 8 percent.

4.2.4 Diffuser Length

A basic assumption in the general performance analysis is that the diffuser length is sufficient to produce one-dimensional flow at its exit. This assumption is verified by the previously presented data for a diffuser length-to-diameter ratio of 10 from the nozzle exit plane. Experimental diffuser pressure distributions with and without the test body are compared in Fig. 12. The diffuser pressures were measured along the top of the diffuser corresponding to the leeward side of the test body. The test body was in its upper position at 11 deg angle of attack with the inlet open. Figure 12 shows that for the same overall pressure ratio, p_B/p_{t_N}, the diffuser pressure recovery is greatly increased by the presence of the test body. However, these data are for the overall pressure ratio required for starting and breakdown. If the diffuser system is over-pressurized, then the diffuser pressure distributions with and without the test body tend to become similar. Operating the diffuser in an over-pressurized condition may be required, in a practical test, to sufficiently reduce the external pressure at the engine exit to allow proper engine operation. Although the data presented in Fig. 12 are for only one test body configuration, similar results were obtained for all configurations.

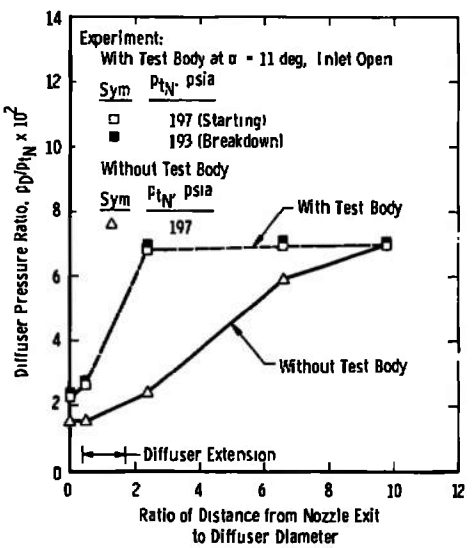

Figure 12. Diffuser pressure distribution.

4.2.5 Test Body Support Strut Leak

The test body support strut passes through the diffuser extension as shown in Fig. 4. All of the data previously presented were obtained with the support strut/diffuser junction sealed in order to obtain maximum diffuser performance. If a leak exists, the effect on diffuser performance can be very large, in the form of drag, and can thus produce

diffuser choking. This drag effect results from a double loss of momentum since the mass flow leaked loses its original momentum and then must be reaccelerated to be pumped out the diffuser exit.

The effect of a leak on diffuser performance could be analytically predicted by the general performance analysis if the leaked mass were known. Unfortunately, the leaked mass flow cannot be realistically estimated at the present time because of the complexity of the flow field and the unusual geometry of the leak flow area.

In practice, it is desirable to have a leak area at the strut/diffuser junction since this simplifies the mechanical design and allows the measurement of forces acting on the test body if required. Experiments were conducted with two leak areas of 0.9 and 6.4 percent of the diffuser cross-sectional area. The experimental results are compared in Fig. 13 and show that both leak areas produce a measurable effect on diffuser performance. The nozzle total pressures for starting corresponding to leak areas of 0.0, 0.9, and 6.4 percent are 200, 200, and 211 psia, respectively. The corresponding nozzle total pressures for breakdown are 197, 195, and 201 psia. These results show that a leak area of 0.9 percent essentially has no effect on the starting and breakdown nozzle total pressures. However, for a leak area of 6.4 percent the nozzle total pressure is increased for starting by 5.7 percent and for breakdown by 2.2 percent.

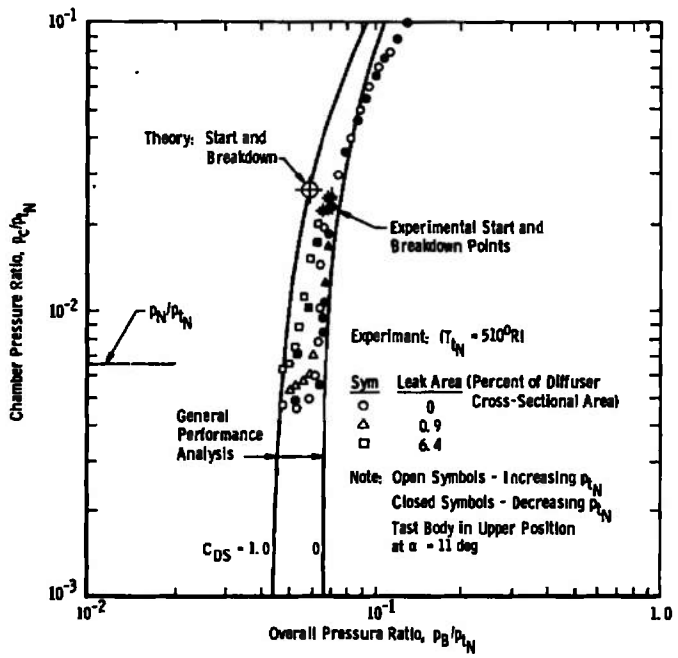

Figure 13. Effect of test body support strut leak on general diffuser performance.

5.0 CONCLUSIONS

The major conclusions from this study are as follows:

1. Diffuser starting and breakdown conditions are determined by the position of the test body, the test chamber pressure feedback in the nozzle boundary layer, and the total drag force. The test body inlet should be located within the test rhombus determined by the nozzle boundary-layer separation pressure ratio to obtain maximum altitude simulation.

2. Extending the diffuser over the test body significantly reduced the minimum test chamber pressure. All configurations tested with a diffuser extension started. The one configuration tested without a diffuser extension did not produce a low enough chamber pressure to become started.

3. The diffuser extension apparently reduces the wave drag of the test body for all configurations tested.

4. The theoretical overall pressure ratio for starting and breakdown was conservative by about 16 percent for all configurations tested except for the one that exhibited a hysteresis. The theory was conservative by about 24 percent for that configuration.

5. The pressure recovery through the diffuser is significantly improved by the test body.

6. Leakage at the test body support strut/diffuser junction can significantly affect diffuser performance. Experimental results show no effect on diffuser performance for a leak area of 0.9 percent of the diffuser cross-sectional area; however, for a leak area of 6.4 percent the nozzle total pressure is increased by 5.7 percent for starting and by 2.2 percent for breakdown.

REFERENCES

1. Bauer, R.C., Matkins, E.H., Barebo, R.L., and Armstrong, W.C. "A Theoretical and Experimental Study of a Jet-Stretcher Diffuser System." Journal of Spacecraft and Rockets, Vol. 10, No. 6, June 1973, pp. 395 - 405.

2. German, R.C., Bauer, R.C., and Panesci, J.H. "Methods for Determining the Performance of Ejector-Diffuser Systems." Journal of Spacecraft and Rockets. Vol. 3, No. 2, February 1966, pp. 193-200.

3. Zukoski, E.E. "Turbulent Boundary-Layer Separation in Front of a Forward-Facing Step." AIAA Journal, Vol. 5, No. 10, October 1967, pp. 1746-1753.

4. Tucker, M. "Approximate Turbulent Boundary-Layer Development in Plane Compressible Flow Along Thermally Insulated Surfaces with Application to Supersonic-Tunnel Contour Correction." NACA TN 2045, March 1950.

5. Weilerstein, Gertrude. "The Addition of Secondary Shock Capability and Modification to the GASL Three-Dimensional Characteristics Program, Part II. User's and Programmer's Manual." GASL TR-653, Part II (AD666742), August 1967.

6. Tinsley, C.R. "Research and Development Testing of Yttria/Rare Earth Stabilized Zirconia Bricks in the Pilot Test Unit (PTU) at AEDC." AEDC-TR-72-161 (AD751298), November 1972.

APPENDIX A
SAMPLE CALCULATION

As a sample calculation, the analysis is applied to the experimental configuration described in Fig. 4. Since the computer program used is for the more comprehensive analysis presented in Ref. 1, many of the input parameters will have fictitious values selected to avoid singularities in the equations. The major assumptions required to apply the comprehensive analysis to the system of interest in this study are presented below, and the parameters used are defined as follows:

A	Area
A_B	Cross-sectional area of diffuser
A_{BE}	Diffuser exit area including blockage
A_S	Total reference area for drag
D	Diameter
k	Ratio of mass flow to nozzle mass flow
L	Diffuser gap (Fig. 1)
ℓ	Length of cylindrical diffuser (Fig. 1)
q	Dynamic pressure
r_N	Radius of nozzle exit
r_j	Radius of jet stretcher inlet
X_j	Distance from nozzle exit to jet stretcher inlet

SUBSCRIPTS

b	Base region
E	External region

i Engine inlet on test body

j Radial gap between nozzle exit and jet-stretcher inlet

P Jet-stretcher porous wall

l Test body engine exit

SUPERSCRIPT

* Nozzle throat region

MAJOR ASSUMPTIONS

1. The flow conditions and area of control volume surface 2 equal the facility nozzle exit flow conditions and area. Therefore,

$$\frac{A_2}{A_N^*} = \frac{A_N}{A_N^*}$$

2. The nozzle flow exterior to the jet stretcher must be zero.

3. The ratio of chamber pressure, p_c, to nozzle exit pressure, p_N, for starting equals the Mach number, M_2 or M_N.

Based on these assumptions, the computer inputs are as follows:

A. Geometric Parameters

1. $A_1/A_N^* =$ 0.0 (Engine Off)

2. $A_1/A_1^* =$ 1.0 (Fictitious)

3. $A_2/A_N^* =$ 10.72 (to make $M_2 = 4.0$)

4. $L/D_B =$ 0.399

5. $A_B/A_N^* =$ 20.472

6. $A_i/A_N^* =$ 0.0 (Engine Off)

7. $A_S/A_N^* =$ 4.713 (A_S is total frontal area of test body and support strut)

8. $A_{b_1}/A_N^* = 0.0$

9. $A_{b_2}/A_N^* = 0.0$

10. $A_3/A_N^* = 7.835$

11. $A_{BE}/A_N^* = 20.472$

12. $r_j/r_N = 0.8$ (fictitious - no jet stretcher)

13. $X_j/r_N = -1.0$ (fictitious - no jet stretcher)

B. Thermodynamic Parameters

1. $T_{t_1}/T_{t_N} = 1.0$ (fictitious - engine off)

2. $T_{t_2}/T_{t_N} = 1.0$

3. $T_{t_p}/T_{t_N} = 1.0$ (fictitious - no jet stretcher)

4. $T_{t_E}/T_{t_N} = 1.0$ (fictitious - no external bleed)

5. $T_{t_j}/T_{t_N} = 1.0$ (fictitious - no jet stretcher)

6. $C_{p_1}/C_{p_N} = 1.0$ (fictitious - engine off)

7. $C_{p_2}/C_{p_N} = 1.0$

8. $C_{p_P}/C_{p_N} = 1.0$

9. $C_{p_E}/C_{p_N} = 1.0$ (fictitious - no external bleed)

10. $C_{p_j}/C_{p_N} = 1.0$ (fictitious - no jet stretcher)

11. $\gamma_1 = 1.4$ (fictitious - engine off)

12. $\gamma_2 = 1.4$

13. $\gamma_N = 1.4$ (fictitious - no facility nozzle)

14. $\gamma_P = 1.4$ (fictitious - no jet stretcher)

$C_{pN} = \gamma_N = 1.7530$

15. γ_E = 1.4 (fictitious - no external bleed)

16. γ_j = 1.4 (fictitious - no jet stretcher)

C. Fluid Mechanical Parameters

1. p_{t_1}/p_{t_N} = 0.0 (engine off)

2. p_{t_2}/p_{t_N} = 1.0

3. p_{b_1}/p_2 = 0.0

4. k_E = 0.0001 (fictitious - no external bleed)

5. k_P = 0.0 (no jet stretcher)

6. C_{DS} = 0.0, 1.0

7. M_N = 4.0

8. p_{t_N} = 100 psi

9. δ_N/r_N = 0.2 (fictitious)

10. δ_N^*/r_N = 0.2 (fictitious)

APPENDIX B
BASIC PTU FACILITY

1.0 GENERAL

The Pilot Test Unit (PTU) is a high-pressure, high-temperature stored heater system capable of providing test air with stagnation pressures and temperatures of 2000 psia and 4500°R, respectively. Initially the PTU was utilized for research testing of high-temperature ceramics; however, the program direction was altered in mid-1971 to reflect a reconfiguration of the PTU to permit model testing. Existing hardware was modified as required, and additional hardware was designed and fabricated or procured. The test hardware included a heater exit air restrictor nozzle plug valve/air-mixer assembly, air-mixer instrument rake, Mach 3 and 4 free-jet nozzles, a subscale chin inlet missile with support strut, exhaust diffuser assembly, test enclosure, and exhaust duct. In addition, new yttria-stabilized zirconia matrix refractories were procured. A schematic of the overall test configuration is presented in Fig. B-1, and a detailed technical report describing the PTU facility and all PTU testing before reconfiguration of the facility is presented in Ref. 6.

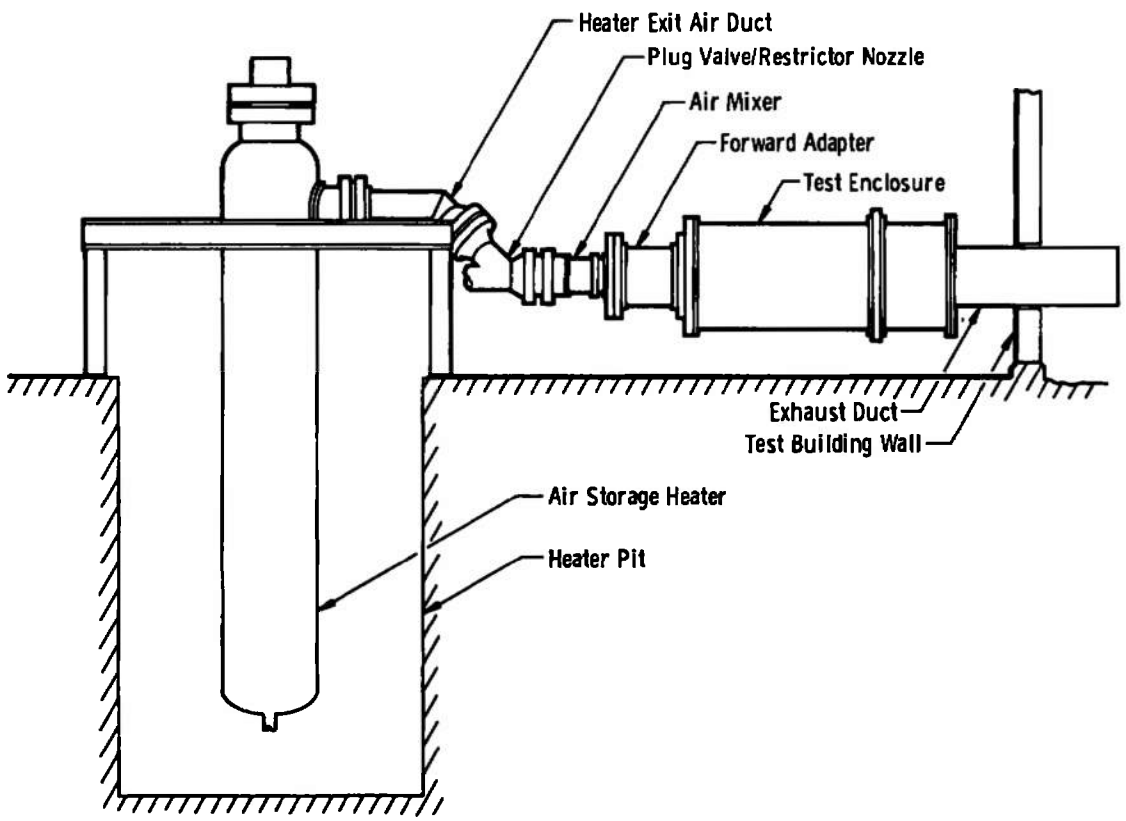

Figure B-1. Overall PTU test configuration.

Shakedown of the facility in the new model test configuration consisted of fourteen hot-flow tests (Tests 101 through 114) and was completed early in November 1972. The test hardware configuration for the shakedown tests is presented schematically in Fig. B-2a.

Chin inlet missile test hardware (with the exception of the test model) was installed following the shakedown tests and is shown schematically in Fig. B-2b. The chin inlet missile test program consisted of 13 hot-flow tests (Tests 115 through 127) completed early in December 1972, the first four of which were accomplished without the chin inlet model installed to obtain facility baseline data.

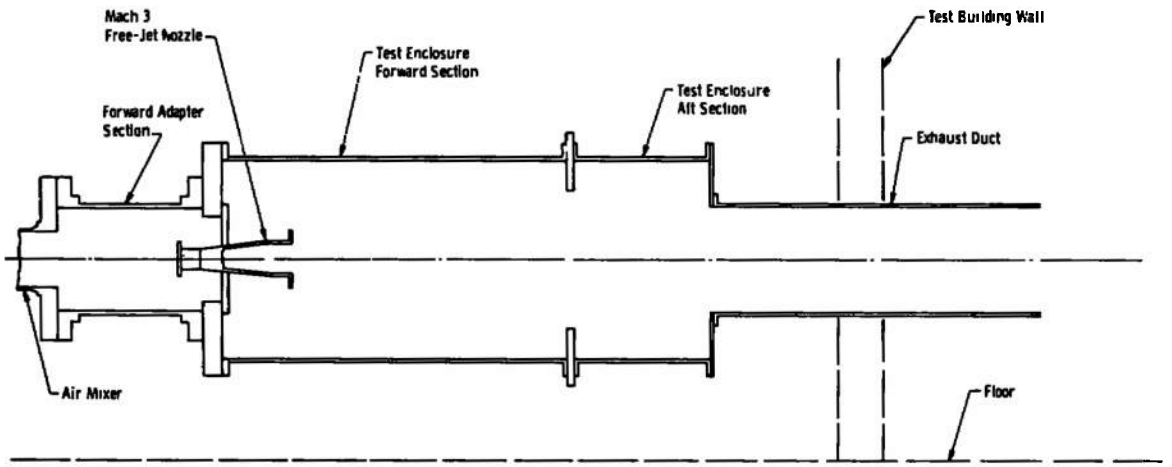

a. Shakedown tests

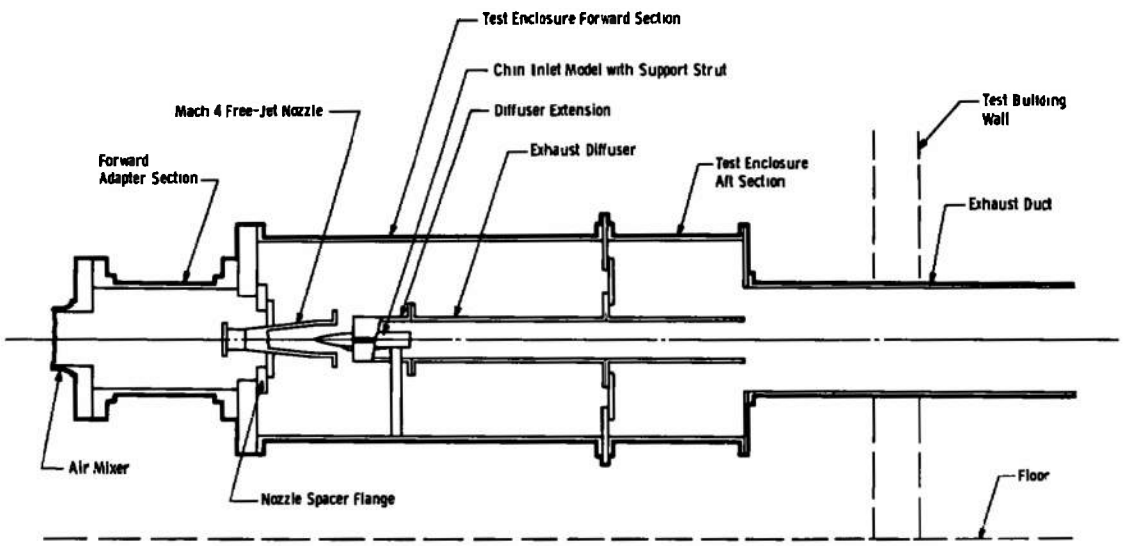

b. Subscale chin inlet tests

Figure B-2. Schematic of test hardware.

Basic hardware performance during both the shakedown and chin inlet missile tests is discussed in the following paragraphs. Pertinent statistics for the tests are presented in Table B-1.

TABLE B-1
TEST SUMMARY

Test Number	Test Date	Run Time, sec	Initial Maximum Heater Temperature, °R	Heater Pressure, psia	Free-Jet Nozzle Total Temperature, °R	Free-Jet Nozzle Total Pressure, psia
101	10-4-72	0	3500	← Unsuccessful Run →		
102	10-20-72	45	3500	1000	1000	100
103	10-23-72	30	3500	1500	1500	175
104	10-24-72	130	3500	500	1000	50
105	10-24-72	70	3500	850	1000	100
106	10-25-72	80	3500	500	1000	150
107	10-25-72	40	3500	1000	1500	175
108	10-25-72	100	3500	550	1000	50
109	10-26-72	40	3500	1000	1000	100
110	10-26-72	30	3500	1500	1100-1300	125
111	10-26-72	90	4000	550	1100-1200	50
112	11-2-72	140	4000	500	1100-1200	50
113	11-2-72	60	4000	1000	1100-1200	100
114	11-2-72	150	4000	100-700	600-1200	50
115	11-30-72	60	4000	500-1000	1200-1300	160-330
116	11-30-72	90	4000	650-1250	1100-1300	190-360
117	11-30-72	80	4000	650-1250	1200-1500	190-360
118	12-1-72	80	4000	350-1500	1000-1400	130-410
119	12-1-72	120	4000	650-1600	1200-1500	180-430
120	12-4-72	100	4000	500-1500	1100-1500	190-430
121	12-4-72	120	4000	500-1200	1200-1400	180-390
122	12-4-72	110	4000	600-1400	1100-1500	190-420
123	12-7-72	100	4000	600-1400	1100-1500	150-360
124	12-7-72	120	4000	600-1200	1200-1400	160-370
125	12-7-72	100	4000	600-1300	1200-1400	190-390
126	12-8-72	110	4000	650-1300	1100-1500	170-480
127	12-8-72	120	4000	650-1200	1100-1400	180-360

2.0 FACILITY PERFORMANCE

2.1 Plug Valve

The restrictor nozzle plug valve and actuator system utilized previously existing hardware provided by FluiDyne Engineering Corporation under contract with the Air Force. The FluiDyne hardware was modified at AEDC to (1) meet the PTU functional and spatial requirements, (2) operate at the maximum heater conditions of 2000 psia and 4500°R, and (3) be integrated into a plug valve/air mixer assembly. Overall operation of the plug valve during the test program as a test air flow intermitter was successful. However, several minor operational difficulties were experienced.

During the initial hardware shakedown tests, the plug valve failed to open with certain combinations of heater pressure and plug valve actuation hydraulic pressure. However, the problem was corrected, and satisfactory plug valve operation was attained. Throughout the shakedown tests and the chin inlet missile test program, a small hot air leak was

present past the plug seat when the air storage heater was pressurized. However, a trickle purge was introduced through the restrictor nozzle film cooling port directly upstream of the plug seat to prevent the hot, high-pressure air from eroding the plug or the plug seat. A schematic of hardware in this area is presented in Fig. B-3.

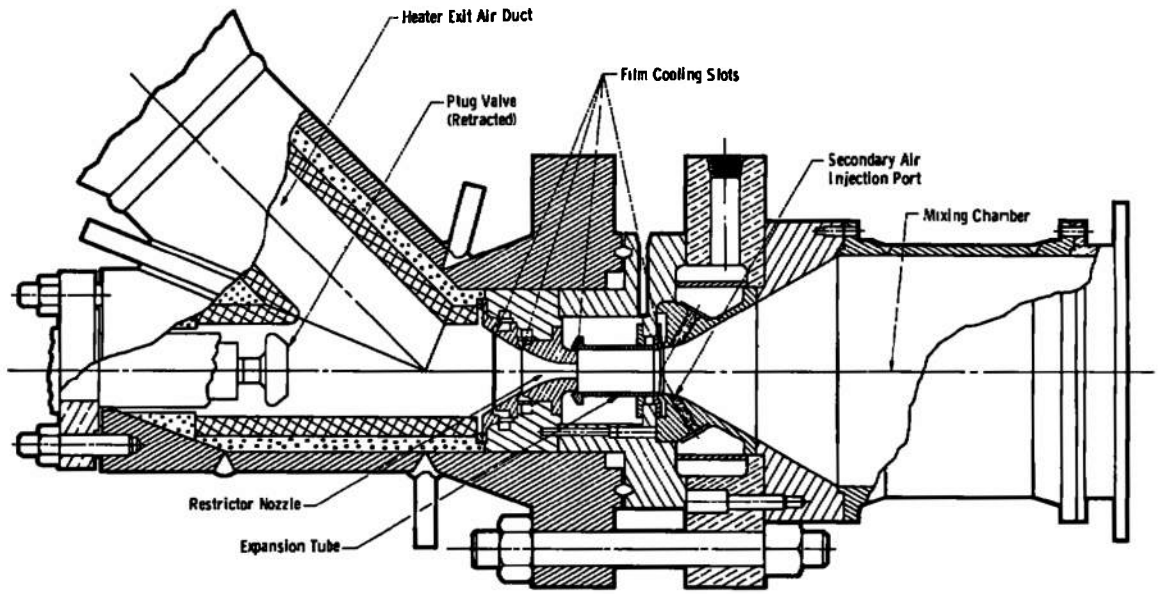

Figure B-3. Integral plug valve/air mixer assembly.

2.2 Air Mixer

The PTU air mixer assembly utilized an existing air mixer, provided by FluiDyne Engineering Corporation under contract with the Air Force, which was modified at AEDC to (1) interface with the plug valve assembly, (2) uprate the mixing chamber operating pressure capability to 400 psi, (3) uprate the secondary air supply manifold operating pressure capability to 1200 psi, and (4) provide instrumentation for analyzing the mixing phenomena. The air mixer assembly is comprised of the plug valve seat/restrictor nozzle, the expansion tube, and a mixing chamber with secondary air injection ports, as is illustrated in Fig. B-3.

Air mixer longitudinal pressure profiles recorded during shakedown testing revealed unexpectedly high pressure levels within the air mixer, particularly in the expansion tube section located immediately downstream of the restrictor nozzle. Typical pressure profiles in this region are presented in Fig. B-4a. A cause of concern was that similar pressures, if encountered in Aerodynamic and Propulsion Test Unit (APTU) testing, would reduce the pressure rating of the APTU low-pressure air mixer. Due to the adverse mixer pressures,

inserts were installed in the eight mixer secondary air injection ports to reduce the blockage of flow from the expansion tube imposed by the secondary air injection jets. The inserts reduced the secondary airflow area by 46 percent and produced a corresponding decrease in blockage area from the jets (assuming no blooming of the jets) of approximately 24 percent. Satisfactory mixer longitudinal pressure profiles were produced. The improvement may be noted by comparing Fig. B-4a with Fig. B-4b. Included in Fig. B-4 are data obtained before the plug valve was opened. These data are presented to illustrate air mixer pressurization resulting only from mixer secondary (cold) airflow and restrictor nozzle film cooling air injected downstream of the closed plug valve. The effects of expansion tube flow blockage as a function of secondary air injection jet size may be noted by comparing the two nondimensionalized pressure plots.

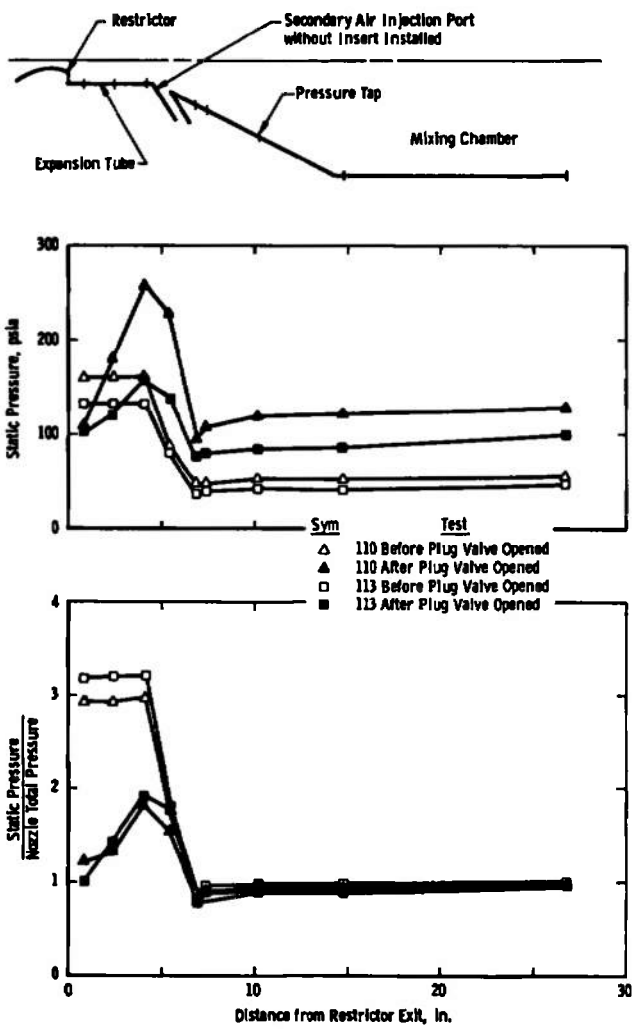

a. Without secondary air injection inserts

Figure B-4. Air mixer longitudinal pressure profiles.

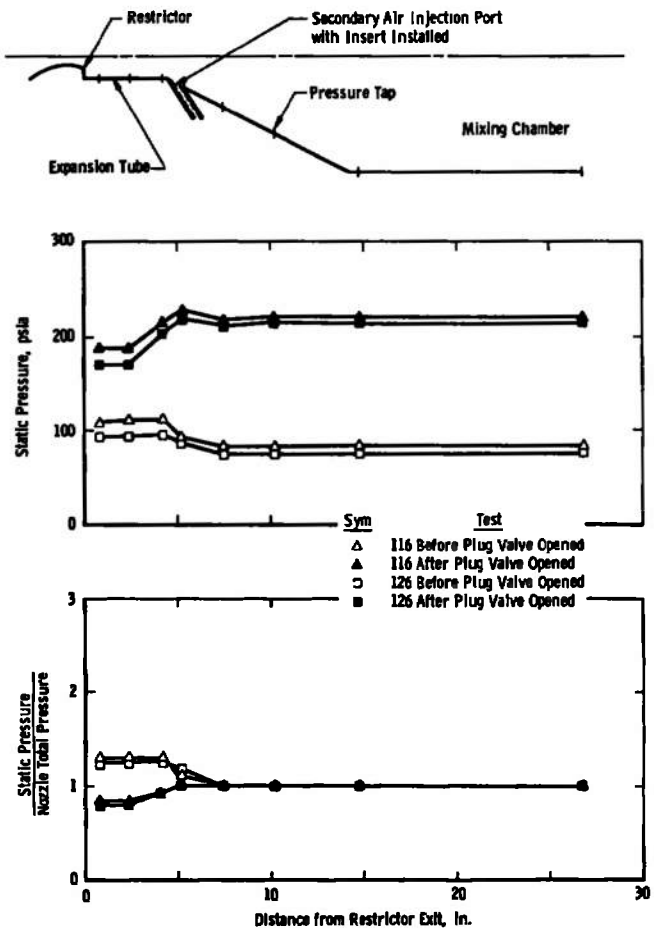

b. With secondary air injection inserts installed

Figure B-4. Concluded.

An instrument rake was utilized at the mixer exit plane to determine if satisfactory mixing of the primary (hot) and secondary (cold) air streams was being accomplished. Mixer exit radial temperature and pressure profiles are presented in Fig. B-5 along with a schematic of the instrument tap configuration. Mixer temperature and pressure profiles remained essentially unchanged after addition of the air injection port inserts.

2.3 Mixer Exit Rake Thermocouples

Four different thermocouple configurations were utilized on the mixer exit rake during the shakedown and chin inlet missile tests. They consisted of (1) shielded, exposed tip, (2) shielded, exposed tip with protective strap, (3) shielded, grounded tip, and (4) shielded, grounded tip thermocouples with a protective strap. These configurations are represented schematically in Fig. B-6.

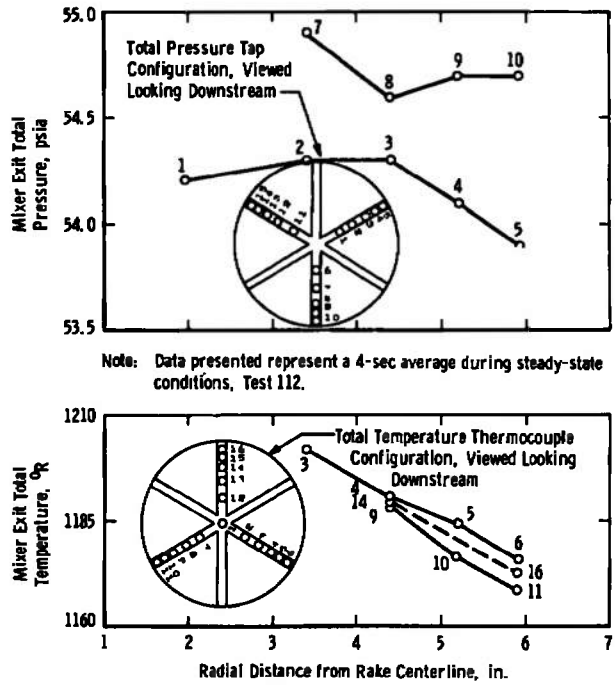

Figure B-5. Mixer exit temperature and pressure profiles.

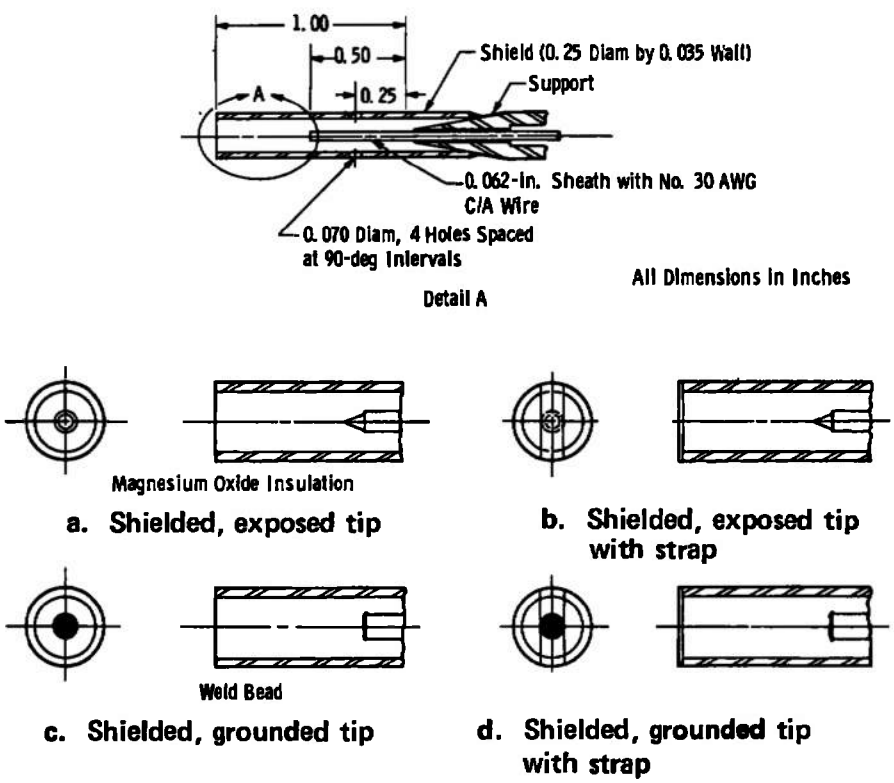

Figure B-6. Mixer exit rake thermocouple configurations.

Initially all rake thermocouples were the shielded, exposed tip type; however, these proved to be unacceptable early during the shakedown tests because of brief surface life due to particle impingement. Therefore, following the first hot-flow shakedown test, the faulty thermocouples were replaced, and protective straps were added to all (16) thermocouples. Following Test 114, thermocouple No. 1 was changed to the shielded, grounded tip with strap configuration, and Nos. 7 and 8 were changed to the shielded, grounded tip without strap configuration. Thermocouple locations are shown in Fig. B-5. Service life of the four types of thermocouples is summarized as follows:

1. Shielded, Exposed Tip:

   After 16 cold-flow tests, 4 out of the 13 thermocouples which were monitored remained good. After 16 cold-flow tests plus 1 hot flow test, 3 (Numbers 6, 12 and 13) out of the 13 thermocouples remained good.

2. Shielded, Exposed Tip with Strap:

   After 13 hot-flow tests, 7 out of the 13 thermocouples remained good. Five of these (Nos. 3, 4, 6, 9, and 12) remained good until the end of the test program (27 hot-flow tests).

3. Shielded, Grounded Tip:

   Two thermocouples were of this type. They remained good from the time of installation until the end of the test program (13 hot-flow tests).

The shielded, exposed tip configuration is considered unacceptable because of the high failure rate of these thermocouples during the shakedown tests; therefore, the sensitivity of the remaining three thermocouple configurations was compared. The data indicated that the shielded, exposed tip with strap configuration exhibited a slightly faster response to temperature transients than the two grounded tip configurations. However, after both sensitivity and useful service life of the three configurations had been considered, the shielded, grounded tip configuration was chosen to be utilized in both the APTU high-pressure and low-pressure air mixer instrument rakes instead of the shielded, exposed tip configuration as originally planned.

2.4 Heater Matrix Refractories

Two minor inspections of the heater matrix refractories were accomplished during the test program. The inspections were conducted after the fourteenth and twenty-seventh

hot-flow tests. During the first inspection, the top two buffer bricks were removed from matrix columns 3 and 4. All four of the bricks contained one or more open cracks and/or fractures. However, fractures of this type are not unusual in the buffer bricks, which are exposed to extreme thermal gradients produced by the burner flame. During the second inspection, the top two bricks were again removed from column 3. However, removal of the top bricks in column 4 was not accomplished because several of the top bricks in this column appeared to be fused together. Instead, the top brick in each of columns 8 and 12 was removed and inspected.

Additional cracks or fracturing was not evident in the column 3 bricks during the second inspection. Overall condition of the bricks inspected from columns 8 and 12 was similar to that of the column 3 bricks. However, white areas were noted on the bricks during the second inspection. The material in these areas remained hard and was not chalky. The top brick from column 12 (manufactured by Zircoa) and the top brick from column 1 (manufactured by Coors) were sent to Wright-Patterson Air Force Base for analysis of the white areas. Testing revealed that (1) the surface of the white area in the Zircoa brick contained 25-percent monoclinic* zirconia, and the yellow surfaces remained cubic, and (2) the Coors brick remained all cubic. The Metallurgy and Ceramics Research Laboratory at WPAFB stated that a reaction possibly took place with contaminants in the white regions. However, whether the contaminants were internal or external is unknown. A plug valve cooling water leak discovered during heater reheat for Test 123 resulted in the admittance of at least a small amount of water to the heater refractories. However, it is not known if any of the water reached the matrix bricks or if the white areas in the matrix bricks were caused either directly or indirectly by the water leak.

3.0 FACILITY HARDWARE ANOMALIES

Two noteworthy facility hardware anomalies occurred during the shakedown/chin inlet tests. A rupture disk partially opened in the heater burner oxidant supply line during heater regeneration for shakedown Test 115 and resulted in fuel-rich burner operation for about 10 hours. This operating mode damaged the burner injector head and injection ports; however, the damage was repaired without significant delay of the test schedule. During heater reheat for Test 123 the matrix temperature profile was noted to be approximately 200°R cooler than normal. An investigation revealed a plug valve cooling water leak on the face of the plug upstream of the plug seat. The leaking water had filled the heater air exit duct, and at least a small amount of water had entered the heater. A schematic of this region may be noted in Fig. B-3. The plug valve assembly was removed and the leak repaired.

*An explanation of the monoclinic and cubic phases of the zirconia crystalline structure is presented in Ref. 6.

4.0 SUMMARY OF RESULTS AND CONCLUSIONS

Operational techniques utilized in a test facility of this type were defined, and operating experience, valuable to the future operation of APTU, was gained during the shakedown/chin inlet missile tests. Overall facility performance throughout the test program was acceptable and, in general, as predicted. Operation of the plug valve as a test air flow intermitter was successful. Problems associated with plug valve operation and adverse longitudinal temperature profiles in the air mixer were solved, and the integrity of four mixer exit rake thermocouple configurations was evaluated. The decision to alter the thermocouple configuration for the APTU air mixers was based on thermocouple data from the shakedown/chin inlet missile test program. Two minor heater matrix refractory inspections revealed that fractures and some areas of monoclinic crystalline phase content were present in the buffer bricks inspected. However, the overall condition of the matrix cannot be estimated from the condition of these few bricks. The overall success of this test program has proved the PTU to be a valuable asset to AEDC not only as a subscale support facility for APTU, but also as an independent high-temperature, high-pressure facility for both research and user testing.

NOMENCLATURE

C_{DS} Overall drag coefficient

C_p Specific heat at constant pressure

F Force

F_S Total drag force

L Diffuser gap (Fig. 1)

ℓ Length of cylindrical diffuser (Fig. 1)

M Mach number

m Mass flow

p Static pressure

T Static temperature

X Distance from nose of test body

α Test body angle of attack relative to nozzle centerline

γ Ratio of specific heats

δ_N Total boundary-layer thickness at nozzle exit

δ_N^* Boundary-layer displacement thickness at nozzle exit

θ Shock wave angle, Eq. (9)

SUBSCRIPTS

B Diffuser exit (Fig. 1)

BLS Boundary-layer separation

c Chamber region (Fig. 1)

D Diffuser wall

E External region (Fig. 1)

M Test body

MIN Minimum

N Nozzle

S Starting conditions

t Total or stagnation conditions

2 Region upstream of test body (Fig. 1)

3 Diffuser gap region (Fig. 1)